IBRO Reports 8 (2020) 65–75

Contents lists available at ScienceDirect

IBRO Reports

journal homepage: www.elsevier.com/locate/ibror

Neuron-specific knockdown of solute carrier protein SLC25A46a induces locomotive defects, an abnormal neuron terminal morphology, learning disability, and shortened lifespan

Md Saheb Ali[a,b], Kojiro Suda[a], Ryosuke Kowada[a], Ibuki Ueoka[a], Hideki Yoshida[a,*], Masamitsu Yamaguchi[a,*]

[a] Department of Applied Biology, Advanced Insect Research Promotion Center, Kyoto Institute of Technology, Matsugasaki, Sakyo-ku, Kyoto, 606-8585, Japan
[b] Faculty of Agriculture, Bangladesh Jute Research Institute, Manik Mia Ave., Dhaka, 1207, Bangladesh

ARTICLE INFO

Keywords:
dSLC25A46
Drosophila
Neuromuscular junction
Mitochondria
Learning abilities

ABSTRACT

Various mutations in the *SLC25A46* gene have been reported in mitochondrial diseases that are sometimes classified as type 2 Charcot-Marie-Tooth disease, optic atrophy, and Leigh syndrome. Although human SLC25A46 is a well-known transporter that acts through the mitochondrial outer membrane, the relationship between neurodegeneration in these diseases and the loss-of-function of *SLC25A46* remains unclear. Two *Drosophila* genes, *CG8931 (dSLC25A46a)* and *CG5755 (dSLC25A46b)* have been identified as candidate homologs of human *SLC25A46*. We previously characterized the phenotypes of pan-neuron-specific *dSLC25A46b* knockdown flies. In the present study, we developed pan-neuron-specific *dSLC25A46a* knockdown flies and examined their phenotypes. Neuron-specific *dSLC25A46a* knockdown resulted in reduced mobility in larvae as well as adults. An aberrant morphology for neuromuscular junctions (NMJs), such as a reduced synaptic branch length and decreased number and size of boutons, was observed in *dSLC25A46a* knockdown flies. Learning ability was also reduced in the larvae of knockdown flies. In *dSLC25A46a* knockdown flies, mitochondrial hyperfusion was detected in NMJ synapses together with the accumulation of reactive oxygen species and reductions in ATP. These phenotypes were very similar to those of *dSLC25A46b* knockdown flies, suggesting that dSLC25A46a and dSLC25A46b do not have redundant roles in neurons. Collectively, these results show that the depletion of SLC25A46a leads to mitochondrial defects followed by an aberrant synaptic morphology, resulting in locomotive defects and learning disability. Thus, the *dSLC25A46a* knockdown fly summarizes most of the phenotypes in patients with mitochondrial diseases, offering a useful tool for studying these diseases.

Introduction

Solute carriers (SLCs) are the largest family of transporters in humans, consisting of 384 unique sequences of proteins forming 52 distinct SLC families (Hediger et al., 2004; Rask-Andersen et al., 2013). SLC transporters localize to the plasma membrane or intracellular compartment membranes. SLCs control the transportation of various substances, including inorganic ions, purines, nucleotides, amino acids (aa), carbohydrates, fatty acids, neurotransmitters, and drug molecules, through biological membranes (Hediger et al., 2004). Mutational or genetic variant defects in SLCs have been implicated in a number of human diseases, such as diabetes, cancer, psychiatric disorders, and neurodevelopmental disorders (Rask-Andersen et al., 2013).

SLC25 family proteins are commonly localized in mitochondria, which is not the case for other SLC families (Hediger et al., 2004). The characteristic property of SLC25A46 is its capability to interact with Mitofusin2 (MFN2), while the other 46 SLC25 family proteins cannot. Based on aa sequences, the SLC25A46 protein is expected to carry a typical full-sized SLC protein structure, including two Solcar repeats, each containing two transmembrane domains. Consistent with the protein structure and mitochondrial localization of SLC25A46, previous studies also predicted that it functions as a transporter across the mitochondrial outer membrane (Palmieri, 2013). SLC25A46 is strongly expressed in the nervous system (Haitina et al., 2006), and cerebellar atrophy, peripheral neuropathy, and optic atrophy may be caused by dominant or recessive mutations in the *SLC25A46* gene of these patients (Abrams et al., 2015; Charlesworth et al., 2016). In Online Mendelian Inheritance in Man (OMIM) (http:/www.omim.org/entry/616505), this

* Corresponding authors.
E-mail addresses: hyoshida@kit.ac.jp (H. Yoshida), myamaguc@kit.ac.jp (M. Yamaguchi).

https://doi.org/10.1016/j.ibror.2020.02.001
Received 4 December 2019; Accepted 17 February 2020

spectrum of disorders was defined as hereditary motor sensory neuropathy type VIB (HMSN6B), being classified as axonal Charcot-Marie-Tooth (CMT) disease type 2. Mutations in *SLC25A46* cause multiple neuropathies, including optic atrophy, Leigh syndrome, progressive myoclonic ataxia, and lethal congenital pontocerebellary hypoplasia (Charlesworth et al., 2016; Janer et al., 2016; Nelson et al., 2016: Nguyen et al., 2017; Wan et al., 2016).

A previous functional analysis with cultured non-neuronal cells revealed a role for SLC25A46 in mitochondrial fission, which may be mediated by protein networks that are different from the fusion complex of MFN2-Optic atrophy protein1 (OPA1) (Abrams et al., 2015). Recent studies that focused on cultured non-neuronal cell models indicated that SLC25A46 plays additional roles in mitochondrial dynamics by managing contacts between the endoplasmic reticulum (ER) and mitochondria or by regulating the oligomerization of MFN1 and MFN2 (Janer et al., 2016; Steffen et al., 2017). Other experiments using the Purkinje cells of *SLC25A46* knockout mice showed the expected phenotypes, including impaired motility, dysfunctional mitochondria, and optic atrophy (Li et al., 2017). We have also recently reported that *CG5755*, one of *Drosophila* homologs of *SLC25A46*, is regulated by epigenetic modification of histone deacetylase, *Rpd3* (Suda et al., 2019). To date, two distinct pathogenesis in *SLC25A46* mutation was suggested, one is impaired transporter activity and the other is altered molecular interaction with several mitochondrial proteins (Abrams et al., 2018). Nevertheless, the pathological mechanisms of diseases caused by the *SLC25A46* mutation remain unclear and there are currently no effective therapies for CMT accompanied by mitochondrial disorders.

Drosophila is a useful genetic model system for studying various neuropathies (Chow and Reiter, 2017). We and other studies using *Drosophila* models for CMT revealed their usefulness in CMT research (Bharadwaj et al., 2016; Kyotani et al., 2016; Niehues et al., 2016; Storkebaum et al., 2009). We previously identified the *Drosophila CG5755* gene as a human *dSLC25A46* homolog and examined phenotypes of pan-neuron-specific *CG5755* knockdown (Suda et al., 2018); however, another gene, *CG8931* was subsequently found to be more closely related to human *SLC25A46*. The *CG8931* and *CG5755* genes have since been renamed *dSLC25A46a* and *dSLC25A46b,* respectively, in FlyBase (https://flybase.org/reports/FBgn0030717) because CG8931 showed higher homology than CG5755 in aa sequences with human SLC25A46. In the present study, we developed a novel model of *Drosophila* mitochondrial disease targeting the *dSLC25A46a* gene. The development of *Drosophila* models for mitochondrial disease, taking into account the strengths of *Drosophila* as a valuable model organism, may contribute to our understanding of its pathological mechanism. We herein demonstrated that pan-neuron-specific *dSLC25A46a* knockdown resulted in impaired motility in both larvae and adults. An aberrant morphology was also found in *dSLC25A46a* knockdown flies at neuromuscular junctions (NMJs). In knockdown flies, mitochondrial hyperfusion was detected in NMJ synapses together with the accumulation of reactive oxygen species (ROS) and reductions in ATP. The observed phenotypes were very similar to those of *dSLC25A46b* knockdown flies (Suda et al., 2018). Possible roles for *dSLC25A46a* and *dSLC25A46b* in the nervous system will be discussed.

Experimental procedures

Fly stocks

Flies were reared on standard food containing 0.65 % agar, 10 % glucose, 4% dry yeast, 5% cone flour, and 3% rice bran at 25 ˚C. Fly lines carrying *w*; +; *elav-GAL4* (stock number: 8760)*, w; +; UAS-w-IR* stock number: 33,623 were obtained from the Bloomington *Drosophila* Stock Center (BDSC) at Indiana University. The flies used in the present study were backcrossed 6 times with the *w* strain to minimize the effects of the genetic background.

Generation of transgenic flies carrying UAS-CG8931-IR

Regarding the knockdown of *CG8931*, RNAi lines carrying *UAS-CG8931-IR* were generated using the pWIZ RNAi cloning vector (Lee and Carthew, 2003). Two target regions of RNAi selected by dsCheck (http://dsCheck.RNAi.jp/) showed no off-target. Total RNAs from the third instar larval brain lobes of Canton S were prepared using Trizol reagent (Invitrogen) and cDNAs were then synthesized with the PrimeScriptTM RT reagent kit (Takara). A region corresponding to aa residues at the N-terminal region (aa 17 to aa 183) of *Drosophila* CG8931 was amplified by PCR with the set of oligonucleotides CG8931$_{17\text{-}183}$*Xba*I and CG8931$_{17\text{-}183}$*Mlu*I. The amplified DNA fragment was digested with *Xba*I *a*nd *Mlu*I and then integrated into the *Avr*II site of pWIZ to create pWIZ-5′-CG8931, and the same fragment was inserted into the *Nhe*I sites of pWIZ-5′-CG8931 in the opposite direction to create pUAS-CG8931-IR$_{17\text{-}183}$. Therefore, the amplified fragments were inserted in the opposite directions on each side of the *white* intron of the pWIZ vector. Similarly, a region corresponding to aa residues at the C-terminal region (aa 217 to aa 383) of *Drosophila* CG8931 was amplified and inserted in the opposite directions on each side of the *white* intron of the pWIZ vector to create UAS-CG8931-IR$_{217\text{-}383}$. The plasmid DNAs pUAS-CG8931-IR$_{17\text{-}183}$ and pUAS-CG8931-IR$_{217\text{-}383}$ were both verified by digestion with appropriate restriction enzymes followed by agarose gel electrophoresis. Each of these plasmid DNAs was injected into early embryos to establish transgenic flies carrying *UAS-dSLC25A46a-IR*$_{17\text{-}183}$ or *UAS-dSLC25A46a-IR*$_{217\text{-}383}$. P element-mediated germ line transformation was performed as previously described (Takahashi et al., 1999). F1 transformants were obtained based on *white* eye color rescue (Takahashi et al., 1999). While 11 fly lines carrying *UAS-CG8931-IR*$_{17\text{-}183}$ or 8 fly lines carrying *UAS-CG8931-IR*$_{217\text{-}383}$ were successfully established, flies carrying the second chromosome insertion and showing the strongest effect on *white* eye color rescue were selected for further experiments.

The oligonucleotides used were as follows.

CG8931$_{17\text{-}183}$*Xba*I 5′-CATGCTCTAGAAACGCACGATGATCACCTGGG-3’

CG8931$_{17\text{-}183}$*Mlu*I5′-CGTACACGCGTGCACCGTTTCGACGAGAGAAGC-3’

CG8931$_{217\text{-}383}$*Xba*I5′-CATGCTCTAGAACCAGCCTGGGCTCTAATCG-3’

CG8931$_{217\text{-}383}$*Mlu*I 5′-CGTACACGCGTCTATTCGCTGTGGTGGTCGGTTG-3’

Comparison of human SLC25A46 and Drosophila SLC25A46a and SLC25A46b aa sequences

UniProt was used to retrieve the aa sequences of *Drosophila* SLC25A46a (CG8931) and SLC25A46b (CG5755) (http:/www.uniprot.org). Using FASTA and BLAST, the identities of and similarities in human SLC25A46 and *Drosophila* SLC25A46a were compared. Comparisons of aa sequences between *Drosophila* SLC25A46a and SLC25A46b were performed in the same manner.

Production of a rabbit anti-dSLC25A46 antibody

The dSLC25A46a peptide Cys-CKNSQDGQGGKYQ − OH, corresponding to aa253-aa264 of dSLC25A46a, was conjugated to keyhole limpet hemocyanin and mixed with Freund’s complete adjuvant to provide a suspension. An added residue was the underlined N-terminal residue Cys. The suspension was then subcutaneously injected into a rabbit (Japanese White), which was kept under specific pathogen-free conditions. The rabbit was then boosted once a week for 7 weeks by inoculating an immunogen of the same quality, and terminal bleeding was performed to collect the maximum serum amount (Scrum Inc.).

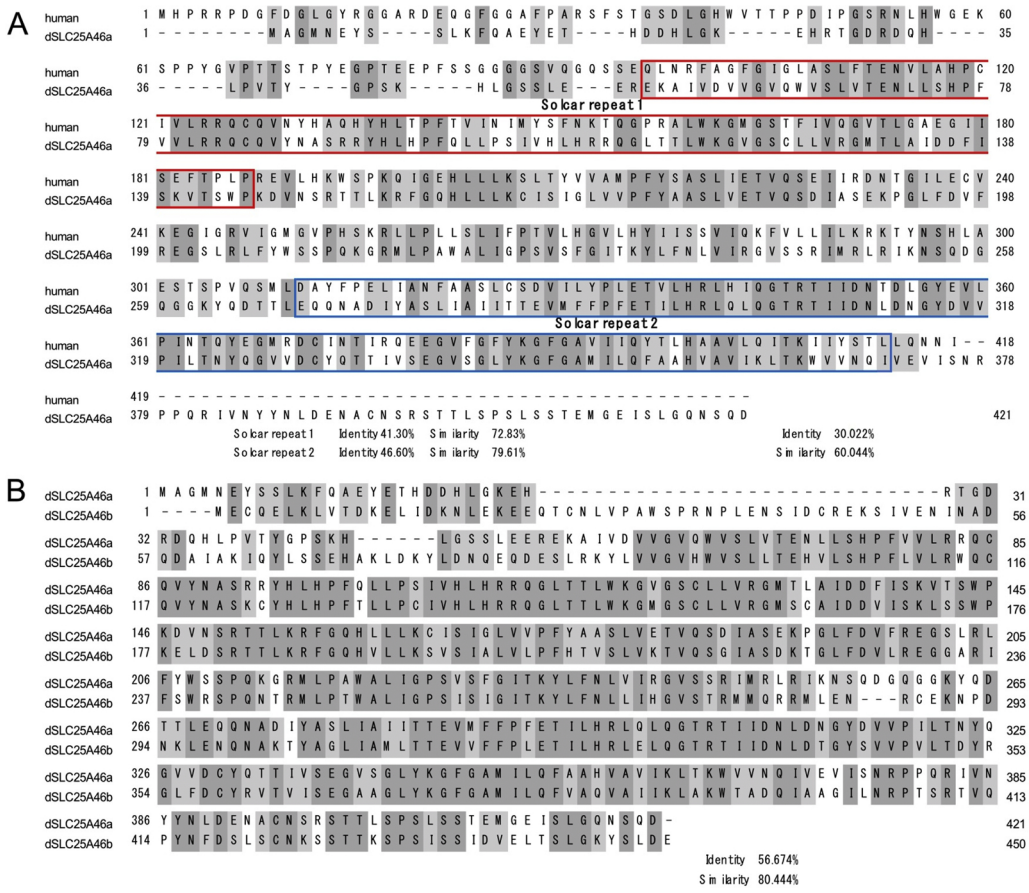

Fig. 1. (A) Sequence alignment of human SLC25A46 with *Drosophila* SLC25A46a. Identical amino acids are darkly shaded and similar or related amino acids are lightly shaded. Solcar repeat 1 and Solcar repeat 2 are boxed with red and blue lines, respectively. (B) Comparison of aa sequences of *Drosophila* SLC25A46a and *Drosophila* SLC25A46a. Identical amino acids are darkly shaded, and similar or related amino acids are lightly shaded.

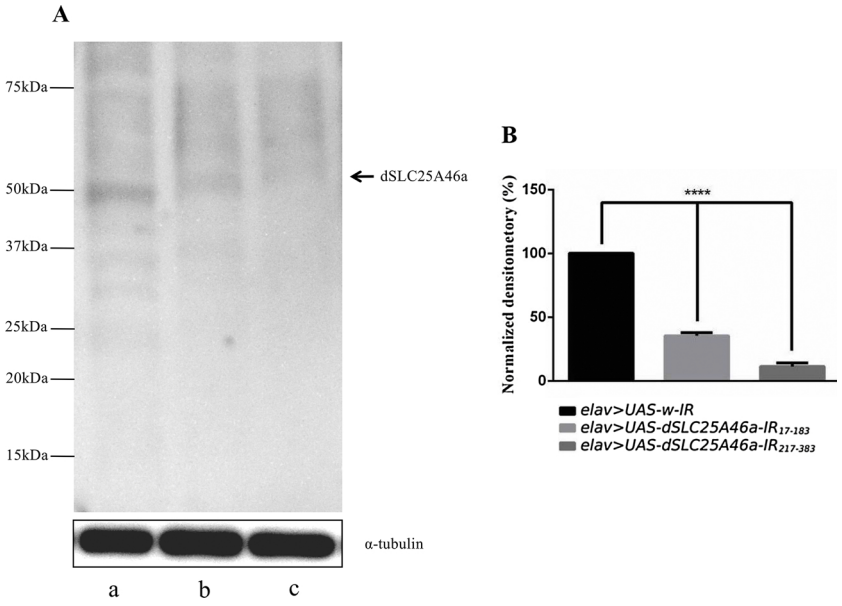

Fig. 2. Knockdown efficiency in larval brains. (A) SLC25A46a protein levels in larval brains analyzed by Western immunoblotting. Proteins were extracted from larval CNS carrying *elav > UAS-w-IR (w; UAS-w-IR/+; elav-GAL4/+) (a), elav > UAS-dSLC25A46a-IR$_{17-183}$ (w; UAS-dSLC25A46a-IR$_{17-183}$/+; elav-GAL4/+) (b), and elav > UAS-dSLC25A46a -IR$_{217-383}$ (w; UAS- dSLC25A46a-IR$_{217-383}$ /+; elav-GAL4/+)* (c). The blotted membrane was probed with a rabbit anti-dSLC25A46a antibody. The band with an apparent molecular mass of 50 kDa corresponding to the dSLC25A46a protein is marked. The positions of size markers are also given on the left. (B) Quantification of the 50-kDa band. α-Tubulin was used as a loading control. The relative intensity of the 50-kDa band normalized to that of α-tubulin is shown as each bar. ****$p < 0.0001$, biological replication, n = 4.

Protein isolation and Western immunoblot analysis

Twenty brain lobes dissected from the larvae of the third instar were homogenized in solution containing 50 mM Tris−HCl pH 6.8, 2% sodium dodecyl sulfate (SDS), 10 % glycerol, 0.1 % bromophenol blue, and 1.2 % β-mercaptoethanol. Homogenates were heated at 95 °C for 5 min. After centrifugation, proteins were separated by electrophoresis on SDS-polyacrylamide gels containing 10 % acrylamide. Proteins were then transferred to polyvinylidene difluoride membranes (Bio-Rad). Blotted membranes were blocked with Tris-buffered saline (TBS) containing 0.1 % Tween-20 and 0.3 % skim milk at 25 °C for 1 h before incubating with rabbit anti-dSLC25A46a serum 1:4000 or mouse monoclonal anti-α-tubulin IgG 1:8000 at 4 °C for 16 h. Membranes were then washed with TBS containing 0.1 % Tween-20 followed by an incubation with horseradish peroxidase-conjugated secondary antibody (GE Healthcare) at a 1:10,000 dilution at 25 °C for 1 h. Protein bands were visualized using ECL Western blotting detection reagents (GE Healthcare) and images were taken and analyzed in the linear range

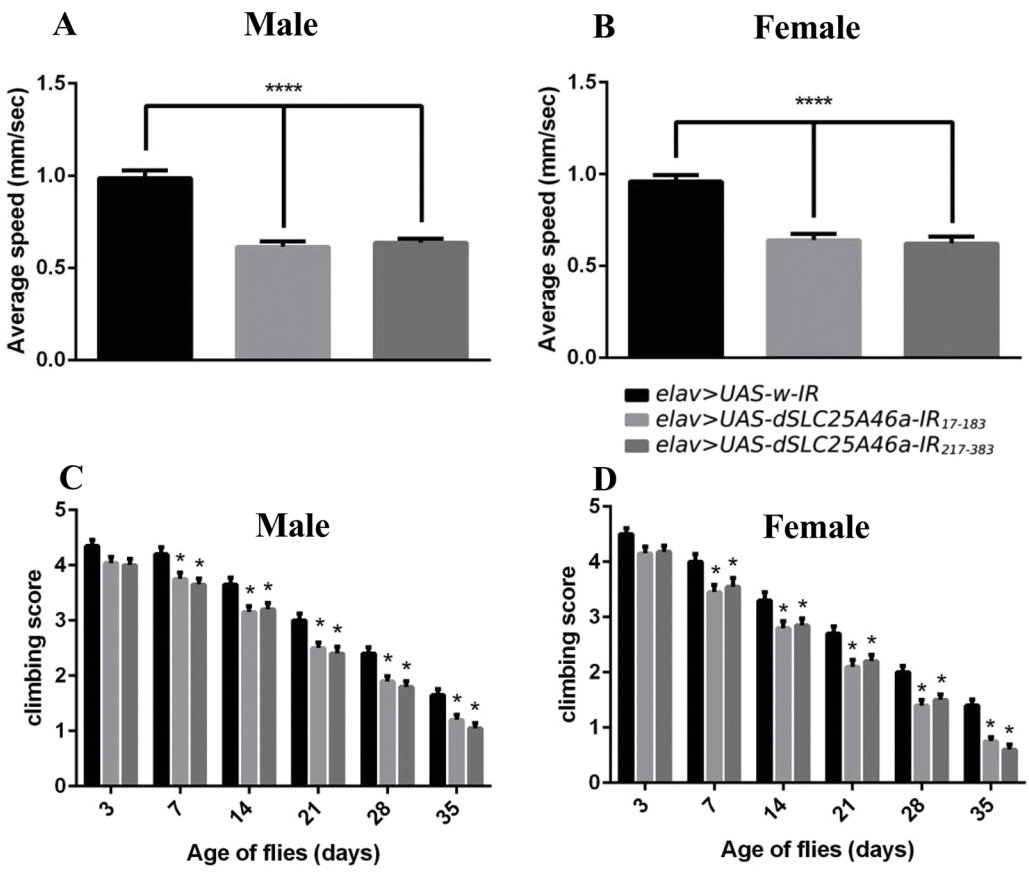

Fig. 3. Locomotor defect in pan-neuron-specific *dSLC25A46a* knockdown flies. (A, B) Larval crawling assay. The pan-neuron-specific knockdown of *dSLC25A46a* causes a decrease in the crawling ability of larvae. Quantified data on the average crawling speed of larvae are shown. (A) Male: *elav > UAS-w-IR* (*w/Y; UAS-w-IR/+; elav-GAL4/+*), *elav > UAS-dSLC25A46a-IR$_{17-183}$* (*w/Y; UAS-dSLC25A46a-IR$_{17-183}$/+; elav-GAL4/+*) *and elav > UAS-dSLC25A46a-IR$_{217-383}$* (*w/Y; UAS- dSLC25A46a-IR$_{217-383}$ /+; elav-GAL4/+*). (B) Female: *elav > UAS-w-IR* (*w/w; UAS-w-IR/+; elav-GAL4/+*), *elav > UAS-dSLC25A46a-IR$_{17-183}$* (*w/w; UAS-dSLC25A46a-IR$_{17-183}$/+; elav-GAL4/+*) *and elav > UAS-dSLC25A46a-IR$_{217-383}$* (*w/w; UAS-dSLC25A46a-IR$_{217-383}$ /+; elav-GAL4/+*). ****$p < 0.0001$. n > 30. (C, D) Adult climbing assay. The pan-neuron-specific knockdown of *dSLC25A46a* causes a decrease in the climbing ability of adult flies. Quantified data on the climbing scores of flies are shown. (A) Male: *elav > UAS-w-IR* (*w/Y; UAS-w-IR/+; elav-GAL4/+*), *elav > UAS-dSLC25A46a-IR$_{17-183}$* (*w/Y; UAS-dSLC25A46a-IR$_{17-183}$/+; elav-GAL4/+*) *and elav > UAS-dSLC25A46a-IR$_{217-383}$* (*w/Y; UAS- dSLC25A46a-IR$_{217-383}$ /+; elav-GAL4/+*). (B) Female: *elav > UAS-w-IR* (*w/w; UAS-w-IR/+; elav-GAL4/+*), *elav > UAS-dSLC25A46a-IR$_{17-183}$* (*w/w; UAS-dSLC25A46a-IR$_{17-183}$/+; elav-GAL4/+*) *and elav > UAS-dSLC25A46a-IR$_{217-383}$* (*w/w; UAS- dSLC25A46a-IR$_{217-383}$ /+ ; elav-GAL4/+*). *$p < 0.05$. n > 100. Technical replication, n = 5.

using AE-9300H Ez-Capture MG (ATTO). The complex of anti-dSLC25A46a IgG and horseradish peroxidase-conjugated secondary antibody was stripped from the membrane before being incubated with anti-α-tubulin IgG (Li et al., 2019).

Crawling assay

The crawling assay was performed with minor modifications as previously described (Nichols et al., 2012). Thirty larvae were collected and washed with PBS in the early stage of the third instar to remove traces of food. Washed larvae at a density of three or four larvae per plate were transferred to agar plates containing 2% agar. Larval motion was captured for 1 min with a digital camera. Using a MOV to AVI converter (Pazera Jacek, Poland), recorded videos were then converted to the AVI type and analyzed using ImageJ (NIH, USA) with a wrMTrck plugin (Nussbaum-Krammer et al., 2015) to track larval motion and draw motion paths (Li et al., 2019; Suda et al., 2018).

Climbing assay

Climbing assays were performed as described previously (Muraoka et al., 2018; Suda et al., 2018). Flies were placed at 28 °C and newly eclosed adult flies were separated and placed in vials at a density of 20 flies per vial. Flies were transferred, without anesthesia, to a conical tube, and were then tapped down at the bottom. Flies were allowed to climb up the wall for 30 s. Flies were then collected at the bottom by tapping the tube, and were again allowed to climb for 30 s. This procedure was repeated five times in total and videotaped. In all climbing assays, the height to which each fly climbed was scored as follows (score (height climbed)): 0 (less than 2 cm), 1 (between 2 and 3.9 cm), 2 (between 4 and 5.9 cm), 3 (between 6 and 7.9 cm), 4 (between 8 and 9.9 cm), and 5 (greater than 10 cm). The climbing index of each fly strain was calculated as follows: the sum of the products of each score multiplied by the number of flies for which that score was recorded, and this number was then divided by five times the total number of flies examined. Climbing assays were performed on days 3, 7, 14, 21, 28, and 35 after eclosion (Li et al., 2019; Suda et al., 2018).

Visualization of synapses and mitochondria at NMJs

The visualization of neurons at NMJs was performed as described previously (Li et al., 2019; Suda et al., 2018). Third instar larvae were dissected in HL3 saline and fixed in 4% paraformaldehyde in PBS at 25 °C for 30 min. After blocking with PBS containing 0.15 % Triton X-100 and 10 % normal goat serum (NGS), mouse anti-Dlg (1:200, DSHB, 4F3) were added to the sample as the detection antibody. Samples were then incubated with anti-mouse IgG labeled with Alexa 594 (1:400) and FITC-conjugated goat anti-HRP IgG (1:200, Jackson ImmunoResearch). After washing, stained samples were mounted in Vectashield (Vector Laboratories) and inspected under a confocal laser scanning microscope (Olympus Fluoview FV10i). MN4 (Ib) in muscle 4 of abdominal segment A2 to A6 was inspected and quantified. Nerve terminal branch lengths were measured using MetaMorph software (Molecular Devices).

To visualize axonal mitochondria at NMJs, GFP targeted to mitochondria were overexpressed (Pilling et al., 2006). Third instar larvae were dissected in HL3 saline and fixed with 4% paraformaldehyde in PBS at 25 °C for 30 min. After washing, samples were blocked with PBS containing 0.15 % Triton X-100 and 10 % normal goat serum NGS at 25 °C for 30 min and incubated with primary antibodies in PBS containing 0.15 % Triton X-100 and 10 % NGS at 4 °C for 16 h. The following antibodies were used as primary antibodies: rabbit anti-GFP IgG (1:200, Medical & Biological Laboratories [MBL], 598) and mouse anti-Dlg

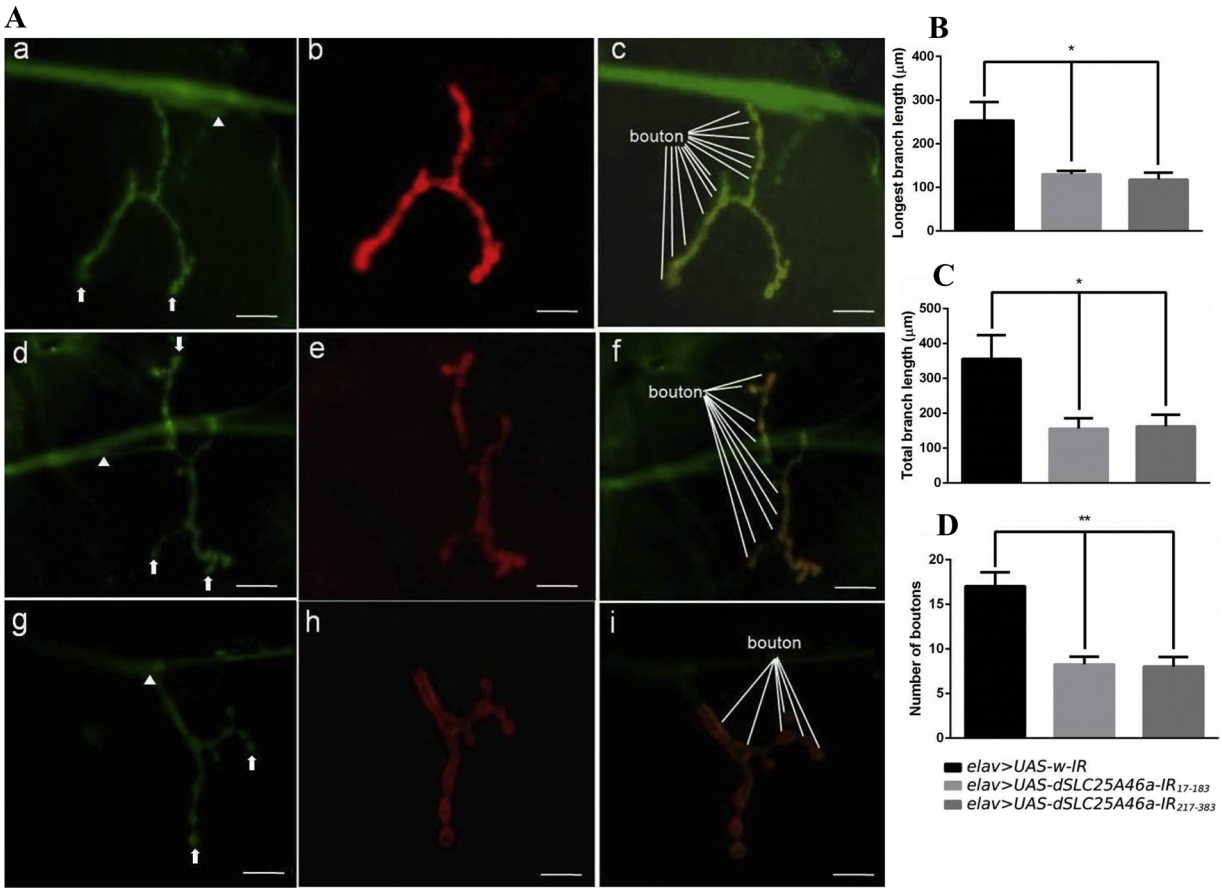

Fig. 4. Knockdown of *dSLC25A46a* in pan-neurons causes an abnormal synapse morphology at NMJs in muscle 4 of third instar larvae. (A) Confocal images showing NMJs stained with anti-HRP IgG (a, d and g) and anti-Dlg IgG (red) (b, e and h). Merged images are shown in panels c, f, and i. The NMJs of flies carrying *elav > UAS-w-IR (w; UAS-w-IR/+; elav-GAL4/+)* (a-c), *elav > UAS-dSLC25A46a-IR$_{17-183}$ (w; UAS-dSLC25A46a-IR$_{17-183}$/+; elav-GAL4/+)* (d-f), and *elav > UAS-dSLC25A46a-IR$_{217-383}$ (w; UAS-dSLC25A46a-IR$_{217-383}$ /+ ; elav-GAL4/+)* (g-i) are shown. The proximal region and distal region of the synapse branch are shown by arrows and arrowheads, respectively. Examples of boutons are marked in panels c, f, and i. Scale bars indicate 20 μm. (B, C, D) Quantified data. In *dSLC25A46a* knockdown larvae, the longest branch length (B) and total length of synaptic branches (C) were shorter and bouton numbers (D) were smaller than control larvae. *$p < 0.05$ and **$p < 0.01$. n = 12.

(1:200, DSHB, 4F3). After being washed with PBS containing 0.3 % Triton X-100, samples were incubated with secondary antibodies labeled with Alexa 594 (1:400) or 488 (1:400) at 25 ˚C for 3 h. After extensive washing with PBS containing 0.3 % Triton X-100, samples were mounted with Vectashield (Vector Laboratories) and inspected under a confocal laser scanning microscope (Olympus Fluoview FV10i). Microscopic images were processed with ImageJ software (NIH) (Li et al., 2019; Suda et al., 2018).

Lifespan assay

Parent flies were placed at 28 ˚C, and newly eclosed adult flies were separated into vials at a low density (20 flies per vial) and maintained in a humidified, temperature-controlled incubator at 28 ˚C and 60 % humidity in a 12-h light/dark cycle. Flies were transferred to new tubes containing fresh food, and dead flies were scored every three days. Survival rates were assessed by the percentage of surviving flies each day until all flies died (Li et al., 2019).

ATP measurement

CellTiter-Glo (Promega) was used to measure ATP levels. The central nervous systems (CNS) of 10 larvae were collected and homogenized in 100 μL of ATP assay buffer (Abcam) and homogenates were centrifuged (13,000 × *g*, 4 ˚C, 5 min). After centrifugation, the supernatant was added to a microtube containing 10 μL of cold trichloroacetic acid (Abcam) and samples were kept on ice for 15 min. After centrifugation at 12,000 × *g* for 5 min, 7.5 μL of neutralization solution (ab204708, Abcam) was added to the sample and left to stand at 0 ˚C for 5 min. Fifty microliters of samples and 50 μL of CellTiter-Glo were mixed in each well. Luminescence was measured using Lumat LB 9507 (Berthold Technologies) (Li et al., 2019).

ROS detection

ROS were detected by CM-H2DCFDA (Thermo Fisher Scientific). Larval CNS in 0.37 % CM-H2DCFDA/PBS was shaken for 15 s. After a 10-min incubation followed by extensive washing with PBS containing 0.005 % NP-40, samples were mounted in Vectashield (Vector laboratories) and immediately inspected by confocal laser scanning microscopy (Olympus Fluoview FV10i) (Li et al., 2019).

Larval learning assay

A larval learning assay was performed as described previously (Jantrapirom et al., 2018). This Pavlovian-type learning assay is based on two steps. A group of larvae is initially exposed to n-amyl acetate AM Millipore, 818700 in the presence of a reward 2 M sucrose, SUC and then 1-octanol OCT Sigma in the absence of SUC. This training is defined as AM+/OCT, with "+" indicating the reward. After this step, reciprocal training is performed. The group of larvae is sequentially exposed to OCT in the presence of SUC and then AM in the absence of

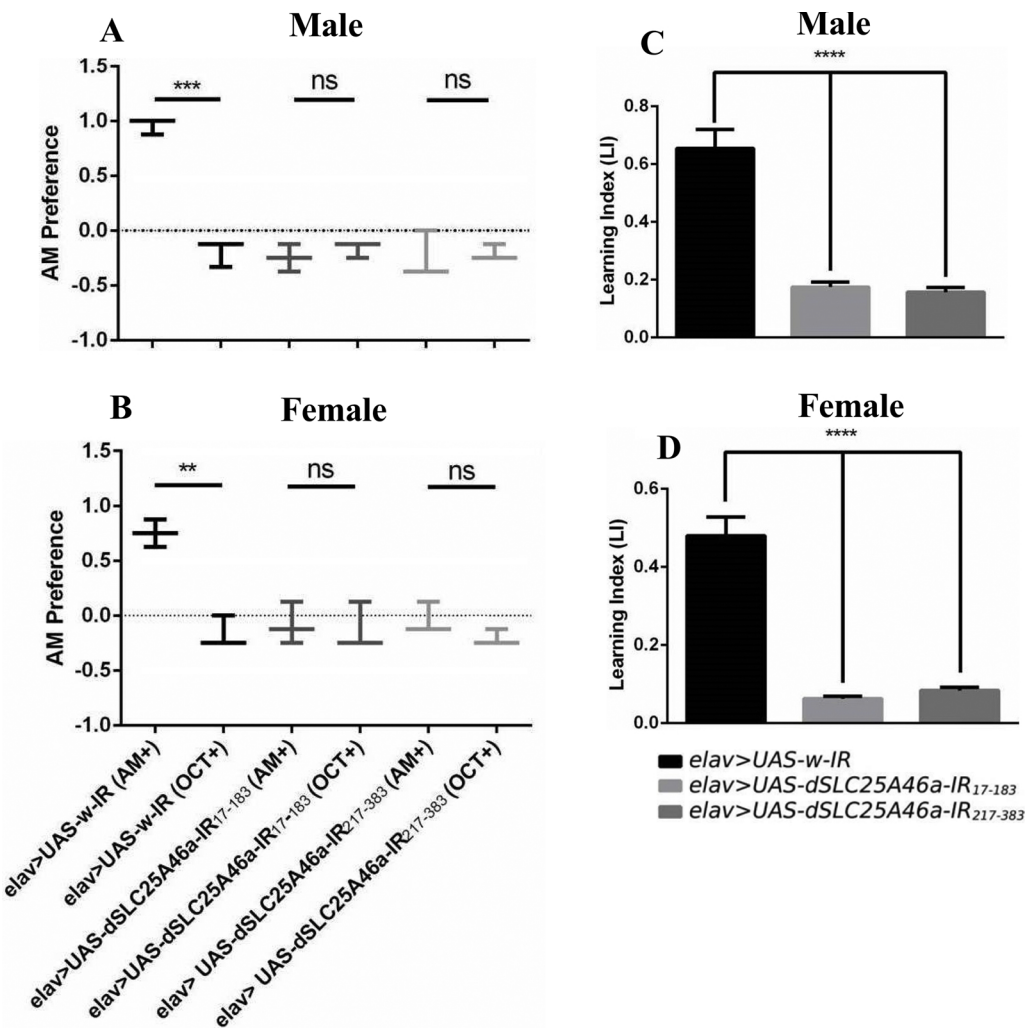

Fig. 5. dSLC25A46a is required for olfactory learning abilities. (A) Male. Larval preference for n-amyl acetate (AM) versus octanol (OCT) (1 = all prefer AM; −1 = all prefer OCT) in larvae carrying *elav > UAS-w-IR* (*w/y; UAS-W-IR/+; elav-GAL4/+*, n = 40), *elav > UAS-dSLC25A46a-IR$_{17-183}$* (*w/Y; UAS-dSLC25A46a-IR$_{17-183}$/+; elav-GAL4/+*, n = 40), and *elav > UAS-dSLC25A46a-IR$_{217-383}$* (*w/Y; UAS-dSLC25A46a-IR$_{217-383}$ /+ ; elav-GAL4/+*, n = 40) 3 min after training on AM/sucrose-containing plates (AM+) or 3 min after training on OCT/sucrose-containing plates (OCT+). ***$p < 0.001$. ns: $p > 0.37$ and ns $p > 0.76$ for male larvae carrying *elav > UAS-dSLC25A46a-IR$_{17-183}$* (*w/Y; UAS-dSLC25A46a-IR$_{17-183}$/+; elav-GAL4/+*, and *elav > UAS-dSLC25A46a-IR$_{217-383}$* (*w/Y; UAS- dSLC25A46a-IR$_{217-383}$ /+; elav-GAL4/+* respectively. Biological replication, n = 3. (C) Normalized AM and OCT learning index for males were averaged for LI. ****$p < 0.0001$ (B) Female: *elav > UAS-w-IR* (*w; UAS-W-IR/+; elav-GAL4/+*, n = 40), *elav > UAS-dSLC25A46a-IR$_{17-183}$* (*w; UAS-dSLC25A46a-IR$_{17-183}$/+; elav-GAL4/+*, n = 40), and *elav > UAS-dSLC25A46a-IR$_{217-383}$* (*w; UAS- dSLC25A46a-IR$_{217-383}$ /+ ; elav-GAL4/+*, n = 40). **$p < 0.01$ and ns: $p > 0.81$ ns $p > 0.14$ for female larvae carrying *elav > UAS-dSLC25A46a-IR$_{17-183}$* (*w; UAS-dSLC25A46a-IR$_{17-183}$/+; elav-GAL4/+*) and *elav > UAS-dSLC25A46a-IR$_{217-383}$* (*w; UAS- dSLC25A46a-IR$_{217-383}$ /+ ; elav-GAL4/+*), respectively. Biological replication, n = 3. (D) Normalized AM and OCT LI for females were averaged for the LI. ****$p < 0.0001$.

SUC. This second training step is defined as OCT+/AM. Five minutes of each training was repeated three times. Ten microliters of each odorant was loaded onto a PCR tube (perforated lid) with 7 holes and placed on the opposite site inside the proper Petri dish. OCT was provided undiluted, while AM was used at a 1:50 dilution with liquid paraffin. Two Petri dishes were used for the training period, one for each couple of odorants. Test Petri dish was divided into two distinct zones with a 1-cm neutral zone arranged in the middle. The neutral zone was defined as the area at which larvae receive the same intensity of each odorant. After training, larvae were tested by exposure to AM and OCT in the absence of SUC. The odorants were deposited on the opposite ends of each Petri dish. Larvae were transferred into a dish 3 min after the training period. Learning ability was evaluated by comparing the preference for the reward odorant against that for the no reward one. The resulting preference indexes are used to calculate the learning index (LI). The AM preference was calculated as: (number of larvae on the AM side-number of larvae on the OCT side)/(total number of larvae on both sides). The AM preference ranges from 1 (perfect attraction to AM) to −1 (perfect attraction to OCT). The normalized AM LI is calculated as: (AM preference-Average of OCT preference)/2. The normalized OCT LI is calculated as: (Average AM preference − OCT preference)/2. The LI is calculated as: (Normalized AM + Normalized OCT)/2 (Li et al., 2019).

Data analysis

GraphPad Prism version 7 was used to statistically analyze data obtained for the crawling assay, the visualization of NMJs, ROS detection, ATP measurements, and learning assays, and p-values were calculated by the unpaired Welch's *t*-test (two-tailed) and for the climbing assay the Two-way ANOVA was used. The p-values were calculated by Dunnett's test. All data are shown as means ± SEM. The Log-rank test in GraphPad Prism version 7 –Survival of Three groups– was used to statistically analyze data obtained for the viability assay.

Results

Comparison of aa sequences among human SLC25A46, Drosophila CG8931, and CG5755

By a BLAST search with human SLC25A46, we previously identified CG5755 as its candidate homolog and named it *Drosophila* SLC25A46 (dSLC25A46) (Suda et al., 2018, 2019). *Drosophila* CG5755 and human SLC25A46 showed 21 % identity and 60 % similarity (Suda et al., 2018). However, another protein, CG8931 was more recently described in FlyBase (https://flybase.org/reports/FBgn0030717). In FlyBase, *CG8931* and *CG5755* are named *Drosophila SLC25A46a* (*dSLC25A46a*)

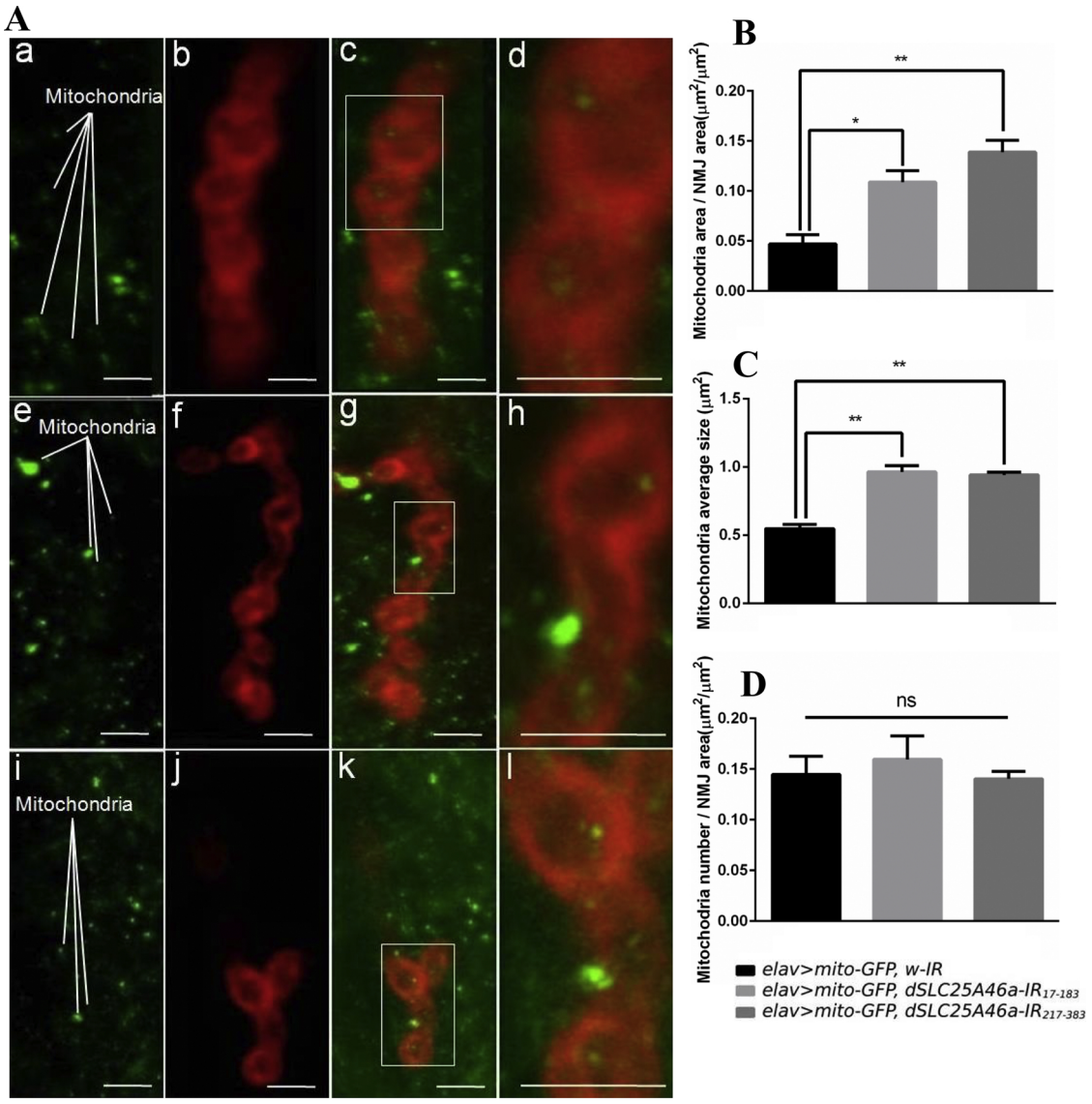

Fig. 6. Knockdown of *dSLC25A46a* causes abnormal mitochondrial dynamics at NMJs in muscle 4 of third instar larvae. (A) Images show NMJs that were double-stained with mito-GFP (green) and anti-Dlg IgG (red). NMJs of flies carrying *w; UAS-w-IR/+; elav-GAL4, UAS-mito-GFP/+* (*a–d*), *w; UAS-dSLC25A46a-IR$_{17-183}$/+; elav-GAL4, UAS-mito-GFP/+* (e–h) and *w; UAS-dSLC25A46a-IR$_{217-383}$ /+; elav-GAL4, UAS-mitoGFP/+* (i–l) are shown. Enlarged images of the region enclosed in panels c, g, and k are shown in panels d, h, and l, respectively. Examples of mitochondria are marked in panels a, e, and i. Scale bars indicate 10 μm. (B-D) Quantified data. In dSLC25A46a knockdown larvae carrying *elav > mito-GFP,dSLC25A46a-IR$_{17-183}$* (*w; UAS-dSLC25A46a-IR$_{17-183}$/+; elav-GAL4, UAS-mito-GFP/+*, n = 12) and *elav > mito-GFP,dSLC25A46a-IR$_{217-383}$* (*w; UAS-dSLC25A46a-IR$_{217-383}$ /+; elav-GAL4, UAS-mito-GFP/+*, n = 12), the area and size of mitochondria significantly differed from (B, C), whereas the number of mitochondria were similar to (D) in control larvae carrying *elav > mito-GFP,w-IR* (*w; UAS-w-IR/+; elav-GAL4, UAS-mito-GFP/+*, n = 12). *$p < 0.05$ and **$p < 0.01$. ns: $p > 0.63$ for larvae carrying *elav > mito-GFP,dSLC25A46a-IR$_{17-183}$* (*w; UAS-dSLC25A46a-IR$_{17-183}$/+; elav-GAL4, UAS-mito-GFP/+*), and ns: $p > 0.83$ for larvae carrying *elav > mito-GFP,dSLC25A46a-IR$_{217-383}$* (*w; UAS-dSLC25A46a-IR$_{217-383}$ /+; elav-GAL4, UAS-mito-GFP/+*).

and *Drosophila SLC25A46b* (*dSLC25A46b*), respectively. Using FASTA and BLAST, the aa sequence of *Drosophila* dSLC25A46a (CG8931) was obtained from UniProt and compared to that of human SLC25 family members and dSLC25A46b (CG5755). dSLC25A46a and human SLC25A46 exhibited 30 % identity and 60 % similarity (Fig. 1A), showing slightly higher homology with human SLC25A46 than dSLC25A46b. dSLC25A46a and other SLC25 subfamily proteins were less closely related. The specific protein domains, Solute carrier (Solcar) 1 and Solcar2 were both strongly conserved between dSLC25A46a and human SLC25A46, showing 41.30 % identity (72.83 % similarity) and 46.60 % identity (79.61 % similarity), respectively (Fig. 1). The Solcar repeat was previously shown to be present in various types of solute carrier proteins involved in the transfer of energy in the inner mitochondrial membrane (Rocha et al., 2018; Traba et al., 2009; Robinson and Kunji, 2006; Klaus et al., 1991). dSLC25A46a and dSLC25A46b showed 57 % identity and 80 % similarity (Fig. 1B). Therefore, both of these genes appear to be paralogs in *Drosophila* and may be an evolutionally equal distance from the human *SLC25A46* gene.

dSLC25A46a knockdown in pan-neurons causes defects in the locomotive ability of larvae and adults

Flies carrying *UAS-CG8931-IR$_{17-183}$* or *UAS-CG8931-IR$_{217-383}$* were crossed by the pan-neuron-specific *elav-GAL4* driver strain and extracts were prepared from larval brain lobes of their progenies. Western immunoblotting with these extracts and an anti-dSLC25A46a antibody was performed to evaluate the efficacy of the knockdown (Fig. 2). A band corresponding to 50 kDa was detected as a single band on the

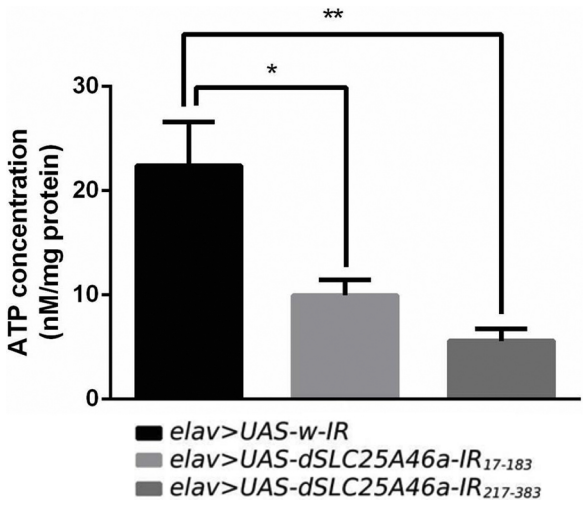

Fig. 7. *dSLC25A46a* knockdown decreases levels of ATP in larval CNS. Quantified data on ATP levels of extracts from the brain lobes of larvae carrying *elav > UAS-w-IR* (*w; UAS-w-IR/+; elav-GAL4/+*), *elav > UAS-dSLC25A46a-IR$_{17-183}$* (*w; UAS-dSLC25A46a-IR$_{17-183}$/+; elav-GAL4/+*), and *elav > UAS-dSLC25A46a-IR$_{217-383}$* (*w; UAS-dSLC25A46a-IR$_{217-383}$ /+; elav-GAL4/+*). In *dSLC25A46a* knockdown larvae, ATP levels were decreased. *$p < 0.05$ and **$p < 0.01$. n = 4.

immunoblot using anti-dSLC25A46a IgG, which recognized the N-terminal region of the dSLC25A46a protein (Fig. 2A). The size of this band was in a similar range of that predicted from the aa sequence of dSLC25A46a (47.36 kDa). The levels of 50-kDa bands in extracts of the brain lobes of larvae carrying *w; UAS-dSLC25A46a-IR$_{17-183}$/+; elav-GAL4/+* and *w; UAS-dSLC25A46a-IR$_{217-383}$ /+; elav-GAL4/+* were 62 % and 85 % lower, respectively, than that of the control larvae carrying *w; UAS-w-IR/+; elav-GAL4/+* (Fig. 2A and B). Therefore, with two independent RNAi lines, we confirmed that *dSLC25A46a* was effectively knocked down.

Larval crawling assays were performed to investigate the effects of the *dSLC25A46a* knockdown on the locomotive ability of larvae (Fig. 3A, B). The *dSLC25A46a* knockdown decreased larval movement speed. Regarding *dSLC25A46a* knockdown larvae carrying *elav > dSLC25A46a-IR$_{17-183}$*, the average crawling speed was 39.30 % lower for males (Fig. 3A) and 33.17 % lower for females than for control larvae carrying *elav > UAS-w-IR* (Fig. 3B). In another RNAi line carrying *elav > UAS-dSLC25A46a-IR$_{217-383}$*, the average crawling speed was 36.73 % lower for males (Fig. 3A) and 35.11 % lower for females (Fig. 3B) than the control larvae carrying *elav > UAS-w-IR*. No significant differences were observed between males and females. Significant reductions were noted in both RNAi lines. Therefore, we observed locomotive defects with two independent RNAi lines targeted to different regions of *dSLC25A46a,* excluding the possible off-target effect.

Adult climbing assays were also performed to investigate the effects of the pan-neuron-specific *dSLC25A46a* knockdown on the locomotive ability of adult flies (Fig. 3C, D). On day 3, slight reductions in climbing ability were observed in both male and female flies carrying *elav > UAS-dSLC25A46a-IR$_{17-183}$* and *elav > UAS-dSLC25A46a-IR$_{217-383}$*. Significant reductions in the locomotive activity of *dSLC25A46a* knockdown flies started on day 7 and locomotive activity then gradually, but continuously decreased each day for both males (Fig. 3C) and females (Fig. 3D), suggesting a relationship with the aging process. It is important to note that in aged day 35 female flies, the climbing abilities of *elav > UAS-dSLC25A46a-IR$_{17-183}$* and *elav > UAS-dSLC25A46a-IR$_{217-383}$* flies were 52 and 44 % that of control *elav > UAS-w-IR* flies (Fig. 3D). These results collectively demonstrated that *dSLC25A46a* plays an important role in locomotive ability.

dSLC25A46a plays a major role in the formation of the NMJ synapse structure in third instar larvae

The results obtained on locomotive defects suggest that *dSLC25A46a* functions in motor neurons. Hence, in *dSLC25A46* knockdown larvae, we examined the morphology of motor neuron presynaptic and post-synaptic terminals at NMJs (Fig. 4A). The *Drosophila* larval NMJ is an established system for the study of synaptic morphology and functions (Keshishian et al., 1996). Larval segmental nerve termini form a series of varicosities at which the muscles are in contact and innervate. This structure, called a bouton, has the stereotyped pattern of a beads-on-a-string structure from which neurotransmitters are released.

The longest synapse branch lengths at NMJs were 57.83 and 46.71 % lower in knockdown flies carrying *elav > UAS-dSLC25A46a-IR$_{17-183}$* and *elav > UAS-dSLC25A46a-IR$_{217-383}$*, respectively, than in control flies carrying *elav > UAS-w-IR* (Fig. 4B). Total branch lengths were significantly shorter in *elav > UAS-dSLC25A46a-IR$_{17-183}$* flies and *elav > UAS-dSLC25A46a-IR$_{217-383}$* flies by 56.23 and 54.33 %, respectively, than in control *elav > UAS-w-IR* flies (Fig. 4C).

Type 1 boutons are glutamatergic and may be divided into type 1b boutons defined as Dlg-positive varicosities with a diameter ≥2 μm, and immature satellite boutons defined as varicosities with a diameter < 2 μm that directly attached to a type 1b bouton (Menon et al., 2013). The numbers of type 1b buttons in knockdown flies carrying *elav > UAS-dSLC25A46a-IR$_{17-183}$* and *elav > UAS-dSLC25A46a-IR$_{217-383}$* were significantly lower at 51.47 and 52.94 %, respectively, that in control *elav > UAS-w-IR* flies (Fig. 4D).

Collectively, these results indicate that *dSLC25A46a* plays an important role in controlling the development and/or maintenance of synapse structures at NMJs, and that locomotive dysfunction may be caused by an aberrant morphology of presynaptic motor neurons and post-synaptic terminals in third instar larvae.

dSLC25A46a knockdown in pan-neurons affects larval learning ability

The synapses of *Drosophila* NMJ are glutamatergic, similar to those in the mammalian CNS (Menon et al., 2013). Therefore, the above-described irregular synapse morphology at NMJs suggests that the depletion of *dSLC25A46a* also affects CNS function. We conducted a *Drosophila* larval olfactory learning assay to investigate the possible role of *dSLC25A46a* in complex neuronal functions in CNS (Jantrapirom et al., 2018). Control larvae demonstrated the ability to correctly associate an odorant with the reward because the preference for the odorant reward was higher than that for the no odorant reward in accordance with training. After training in the presence of AM and SUC (AM+), control larvae carrying *elav > UAS-w-IR* flies showed the ability to recognize the odorant reward in the presence of both odorants (AM+/OCT), while after training in the presence of OCT and SUC (OCT+), both odorants (OCT+/AM) showed a significant preference for OCT (Fig. 5A, B). In larvae carrying *elav > UAS-dSLC25A46a-IR$_{17-183}$* and *elav > UAS-dSLC25A46a-IR$_{217-383}$*, the number of preferred AM was not significantly higher in AM+/OCT than in OCT+/AM (Fig. 5A, B). These results demonstrated that *dSLC25A46a* knockdown larvae were not able to associate the odorant with the reward. The LI clearly showed that larvae carrying *elav > UAS-dSLC25A46a-IR$_{17-183}$* and *elav > UAS-dSLC25A46a-IR$_{217-383}$* had learning abilities that were 73.32 and 76.06 % lower, respectively, for males (Fig. 5C) and 86.95 and 82.06 % lower, respectively, for females (Fig. 5D). These results suggest that *dSLC25A46a* is required for complex neuronal functions in CNS, such as learning.

dSLC25A46a plays a key role in the regulation of mitochondrial dynamics at NMJs in third instar larvae

Previous studies using cultured cells demonstrated that human SLC25A46 affects mitochondrial fission (Abrams et al., 2015).

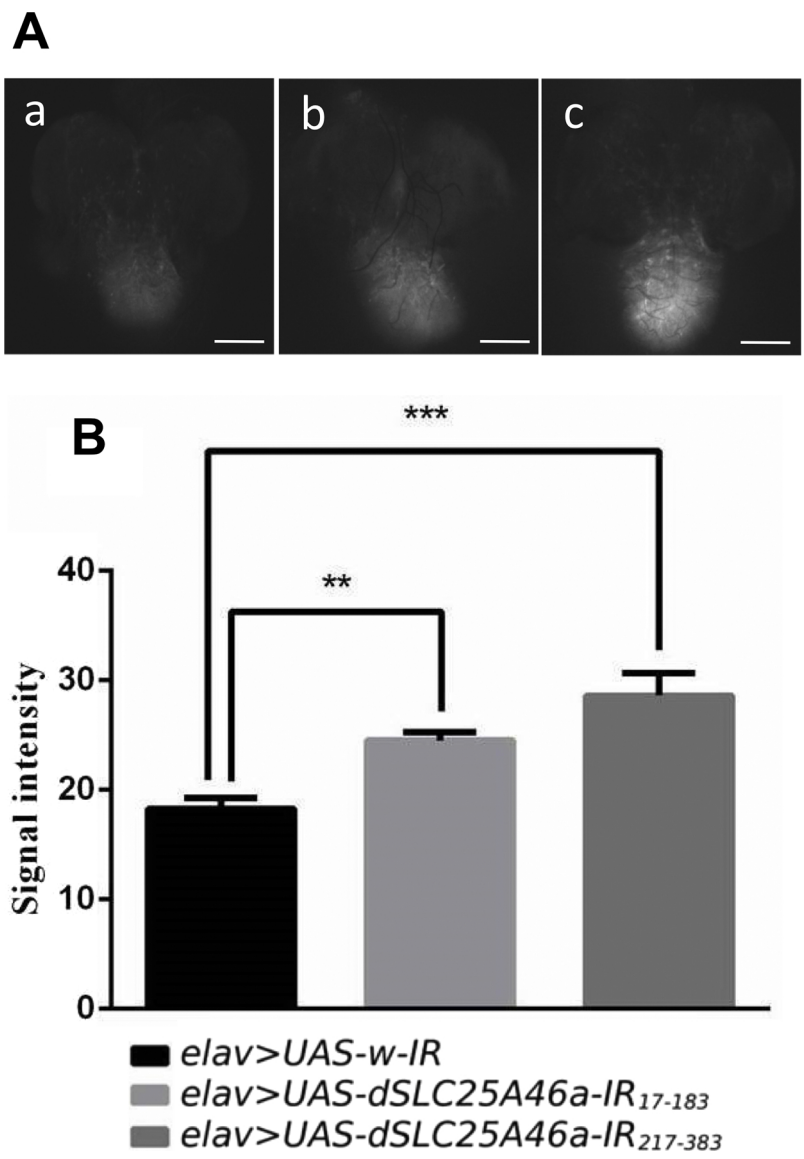

Fig. 8. *dSLC25A46a* knockdown in pan-neurons increases ROS production in the CNS of third instar larvae. (A) Third instar larval CNS stained with CM-H2DCFDA. Images of *elav > UAS-w-IR (w; UAS-w-IR/+; elav-GAL4/+)* (a), *elav > UAS-dSLC25A46a-IR$_{17-183}$* (*w; UAS-dSLC25A46a-IR$_{17-183}$/+; elav-GAL4/+*) (b), and *elav > UAS-dSLC25A46a-IR$_{217-383}$* (*w; UAS- dSLC25A46a-IR$_{217-383}$ /+; elav-GAL4/+*) (c) are shown. Scale bars indicate 100 μm. (B) Quantified data. In *dSLC25A46a* knockdown larvae carrying *elav > UAS-dSLC25A46a-IR$_{17-183}$ (w; UAS-dSLC25A46a-IR$_{17-183}$/+; elav-GAL4/,+*, n = 8) and *elav > UAS-dSLC25A46a-IR$_{217-383}$ (w; UAS- dSLC25A46a-IR$_{217-383}$ /+ ; elav-GAL4/+*, n = 8), ROS signals were stronger than those in control larvae carrying *elav > UAS-w-IR (w; UAS-W-IR/+; elav-GAL4/+*, n = 8). $^{**}p < 0.01$ and $^{***}p < 0.001$.

Therefore, in *dSLC25A46a* knockdown larvae, we examined mitochondrial morphology at NMJs (Fig. 6A). Mitochondria were visualized in NMJs by overexpressing mitochondria-targeted GFP (Pilling et al., 2006). In flies carrying *elav > mito-GFP, dSLC25A46a-IR$_{17-183}$* (Fig. 6A, panels e–h) and *elav > mito-GFP, dSLC25A46a-IR$_{217-383}$* (Fig. 6A, panels i–l), mitochondrial densities were 131.04 and 194.79 % higher, respectively (Fig. 6B), and mitochondrial sizes were also 1.76- and 1.72-fold higher, respectively (Fig. 6C), than those in control larvae carrying *elav > mitoGFP, w-IR* (Fig. 6A, panels a–d). No significant differences were observed in the number of mitochondria between *dSLC25A46a* knockdown flies and control flies (Fig. 6D).

These results suggest that under depleted *dSLC25A46a* conditions, hyperfused or enlarged mitochondria accumulate in NMJs due to the lack of the proper control of mitochondrial dynamics. The aggregation of defective mitochondria in NMJs may lead to neuronal dysfunction and an aberrant morphology of pre-synaptic and post-synaptic motor neuron terminals in third instar larvae.

dSLC25A46a knockdown in pan-neurons reduces the amount of ATP in the CNS of third instar larvae

We assessed the level of ATP as an indication of mitochondrial dysfunction in *dSLC25A46a* knockdown flies. In *dSLC25A46a* knockdown larvae carrying *elav > UAS-dSLC25A46a-IR$_{17-183}$*, the level of ATP decreased to 60.10 % that in control flies carrying *elav > UAS-w-IR* (Fig. 7). The level of ATP in flies carrying *elav > UAS-dSLC25A46a-IR$_{217-383}$* also decreased to 77.68 % that in control flies (Fig. 7). These results suggest that in *dSLC25A46a* knockdown larvae, mitochondrial function is defective. The accumulation of defective mitochondria in NMJs appears to cause neuronal dysfunction and an aberrant motor neuron morphology.

dSLC25A46a knockdown in pan-neurons increases ROS levels in CNS

The results obtained on the mitochondrial aberrant morphology and decreases in ATP levels described above indicate that *dSLC25A46a* plays a role in the function of mitochondria. Therefore, in the larval CNS, we measured the level of ROS, an oxidative stress indicator of mitochondria (Fig. 8). In knockdown flies carrying *elav > UAS-dSLC25A46a-IR$_{17-183}$*, the intensity of the ROS signal increased to 134.16 % (Fig. 8Ab, B) that in control *elav > UAS-w-IR* flies (Fig. 8Aa, B). In flies carrying *elav > UAS-dSLC25A46a-IR$_{217-383}$*, ROS signal intensity increased to 156.57 % that in control flies (Fig. 8Ac, B). These results, take together with decreased ATP levels and an aberrant mitochondrial morphology, suggest that mitochondrial function is impaired in *dSLC25A46a* knockdown flies.

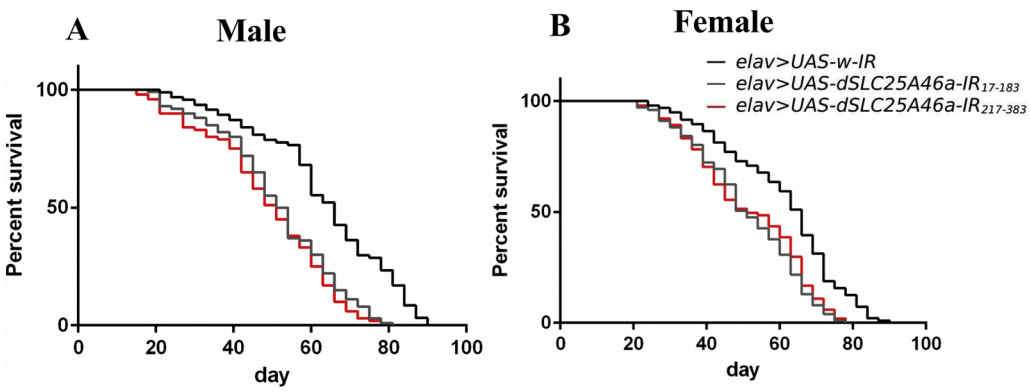

Fig. 9. Knockdown of *dSLC25A46a* in pan-neurons causes a shortened lifespan in adult flies. The survival rates of adult male (A) flies carrying *elav > UAS-w-IR* (*w/y; UAS-W-IR/+; elav-GAL4/+*, n = 100), *elav > UAS-dSLC25A46a-IR$_{17-183}$* (*w/Y; UAS-dSLC25A46a-IR$_{17-183}$/+; elav-GAL4/+*, n = 100), and *elav > UAS-dSLC25A46a-IR$_{217-383}$* (*w/Y; UAS-dSLC25A46a-IR$_{217-383}$ /+ ; elav-GAL4/+*, n = 100) and female (B) flies carrying *elav > UAS-w-IR* (*w/w; UAS-W-IR/+; elav-GAL4/+*, n = 100), *elav > UAS-dSLC25A46a-IR$_{17-183}$* (*w/w; UAS-dSLC25A46a-IR$_{17-183}$/+; elav-GAL4/+*, n = 100), and *elav > UAS-dSLC25A46a-IR$_{217-383}$* (*w/w; UAS-dSLC25A46a-IR$_{217-383}$ /+ ; elav-GAL4/+*, n = 100) are shown.

dSLC25A46a knockdown in pan-neurons shortens the adult fly lifespan

We also examined the effects of the pan-neuron-specific *dSLC25A46a* knockdown on the lifespan of flies. The numbers of surviving knockdown flies carrying *elav > UAS-dSLC25A46a-IR$_{17-183}$* and *elav > UAS-dSLC25A46a-IR$_{217-383}$* and control flies carrying *elav > UAS-w-IR* were recorded until the death of the last fly (Fig. 9). The results obtained showed that 50 % of *dSLC25A46a* knockdown flies carrying *elav > UAS-dSLC25A46a-IR$_{17-183}$* and *elav > UAS-dSLC25A46a-IR$_{217-383}$* died by day 50, while control *elav > UAS-w-IR* flies had a median lifespan of 63 days for both males and females (Fig. 9). Therefore, the pan-neuron-specific *SLC25A46a* knockdown resulted not only in locomotive defects and impaired learning ability, but also in shorter lifespans.

Discussion

Although human SLC25A46 is a well-known transporter that functions through the mitochondrial outer membrane, the pathogenic mechanisms of mitochondrial diseases in which mutations in the *SLC25A46* gene are involved have not yet been elucidated. Analyses of the phenotype induced by the knockdown of its *Drosophila* homolog have provided insights into the underlying pathogenic mechanisms. In the present study, we revealed that neuron-specific *dSLC25A46a* knockdown induced locomotive defects in both the larval and adult stages, motoneuron and mitochondrial defects in NMJs, and learning defects that were accompanied by ROS accumulation and ATP reductions. These results suggest that a decreased *dSLC25A46a* level is the primary cause of mitochondrial dysfunction. A lack of mitochondrial dynamics may result in the accumulation of defective mitochondria with a fused or enlarged morphology. This may then contribute to an aberrant neuronal morphology with neuronal dysfunction in NMJs that ultimately leads to defects in locomotive ability and also complex neuronal functions in CNS, such as learning ability. In contrast, previous studies reported that the depletion of Marf, a *Drosophila* homologue of MFN2, another causative factor for CMT, induced mitochondrial fragmentation rather than mitochondrial fusion accompanied by neuronal defects (Altanbyek et al., 2016; Sandoval et al., 2014). Therefore, the correct regulation of mitochondrial dynamics appears to be essential for proper neuronal function.

We constructed two separate *dSLC25A46a* inverted repeat constructs, such as *UAS-dSLC25A46a-IR$_{17-183}$* and *UAS-dSLC25A46a-IR$_{217-383}$*, to exclude the potential off-target effects of the RNAi constructs used. Target sequences were designed to avoid off-target effects for these two RNAi lines. When crossing these transgenic fly lines with the *elav-GAL4* line to express *dSLC25A46a* dsRNA specifically in neuronal tissues, each independent fly strain showed basically the same phenotype. These results demonstrated that the phenotypes found with neuron-specific *dSLC25A46a* knockdown flies were not due to an off-target effect, but to a reduction in the protein level of *dSLC25A46a*.

We previously reported that the depletion of *dSLC25A46b* impaired motility in both larvae and adults, induced morphological defects in NMJs, such as reduced synaptic branch lengths, decreased the number and size of boutons, and caused mitochondrial defects, such as mitochondrial fusion, the accumulation of ROS, and reductions in ATP levels (Suda et al., 2018). These phenotypes are very similar to the phenotype induced by the knockdown of *dSLC25A46a*. Although dSLC25A46a and dSLC25A46b show high homology at 57 % identity and 80 % similarity, these findings suggest that they may transport different substrates and do not complement the defects induced by the knockdown of each other in neurons. Further analyses are needed to clarify this point. Although the knockdown of *dSLC25A46b* exerted no effects on the lifespans of adult flies (Suda et al., 2018), the knockdown of *dSLC25A46a* effectively shortened their lifespans. Moreover, pan-neuron-specific *dSLC25A46a* knockdown flies carrying two copies of *dSLC25A46a-IR* become lethal (data not shown), while *dSLC25A46b* knockdown flies carrying two copies of *dSLC25A46b-IR* were viable (Suda et al., 2018). Therefore, *dSLC25A46a* may play a more essential role in the viability of flies than *dSLC25A46b*. However, since knockdown efficiency appears to be higher for *dSLC25A46a* RNA lines than *dSLC25A46b* RNA lines, it may simply due to difference in knockdown efficiency.

Our knockdown *Drosophila* model targeting *dSLC25A46a* recapitulates most of the phenotypes in patients with mitochondrial disease, offering a useful tool for researching these diseases. Based on the successful use of *Drosophila* models to identify genetic interactions with genes that cause different neurodegenerative diseases (Azuma et al., 2014; Shimamura et al., 2014; Muraoka et al., 2018), extensive genetic screening with neuron-specific *dSLC25A46a* knockdown flies will enable us to identify genes and signaling pathways associated with *dSLC25A46a* functions in the neuron. Comparative studies with neuron-specific *dSLC25A46b* knockdown flies may also allow us to study the differential roles of these two related transporters. The genes and pathways identified with both *dSLC25A46a* knockdown flies and *dSLC25A46b* knockdown flies may be important targets for mitochondrial disease therapy, including CMT. Therefore, the neuron-specific *dSLC25A46a* knockdown flies established in the present study as well as the *dSLC25A46b* knockdown flies previously established may be useful models in the search for new therapeutic targets for these syndromes as well as candidate therapy substances.

Conflict of interest

The authors declare no competing interests in relation to the work described.

Author statement

M.S. Ali, K. Suda, R. Kowada and I. Ueoka designed and performed the experiments. M.S. Ali, K. Suda, R. Kowada analyzed the data and wrote the manuscript. M. Yamaguchi and H. Yoshida contributed to resources and edited the manuscript. All the authors finally reviewed and approved the manuscript.

Acknowledgments

We thank the Kyoto Stock Center, Bloomington Drosophila Stock Center, and Vienna Drosophila Genetic Resource Center for the fly lines. This research was partially supported by the JSPS Core-to-Core Program, Asia-Africa Science Platforms B (MY), JSPS KAKENHI Grant Number JP19K06659 (MY), and JSPS Invitational Fellowship for Research in Japan [Long-term] (MSA).

References

Abrams, A.J., Hufnagel, R.B., Rebelo, A., Zanna, C., Patel, N., Gonzalez, M.A., Campeanu, I.J., Griffin, L.B., Groenewald, S., Strickland, A.V., Tao, F., Speziani, F., Abreu, L., Schüle, R., Caporali, L., La Morgia, C., Maresca, A., Liguori, R., Lodi, R., Ahmed, Z.M., Sund, K.L., Wang, X., Krueger, L.A., Peng, Y., Prada, C.E., Prows, C.A., Schorry, E.K., Antonellis, A., Zimmerman, H.H., Abdul-Rahman, O.A., Yang, Y., Downes, S.M., Prince, J., Fontanesi, F., Barrientos, A., Németh, A.H., Carelli, V., Huang, T., Zuchner, S., Dallman, J.E., 2015. Mutations in SLC25A46, encoding a UGO1-like protein, cause an optic atrophy spectrum disorder. Nat. Genet. 47, 926–932. https://doi.org/10.1038/ng.3354.

Abrams, A.J., Fontanesi, F., Tan, N.B., Buglo, E., Campeanu, I.J., Rebelo, A.P., Kornberg, A.J., Phelan, D.G., Stark, Z., Zuchner, S., 2018. Insights into the genotype-phenotype correlation and molecular function of SLC25A46. Hum. Mutat. 39 (12), 1995–2007. https://doi.org/10.1002/humu.23639.

Altanbyek, V., Cha, S.-J., Kang, G.-U., Im, D.S., Lee, S., Kim, H.-J., Kim, K., 2016. Imbalance of mitochondrial dynamics in *Drosophila* models of amyotrophic lateral sclerosis. Biochem. Biophys. Res. Commun. 481, 259–264. https://doi.org/10.1016/j.bbrc.2016.10.134.

Azuma, Y., Tokuda, T., Shimamura, M., Kyotani, A., Sasayama, H., Yoshida, T., Mizuta, I., Mizuno, T., Nakagawa, M., Fujikake, N., Ueyama, M., Nagai, Y., Yamaguchi, M., 2014. Identification of ter94, *Drosophila* VCP, as a strong modulator of motor neuron degeneration induced by knockdown of Caz, *Drosophila* FUS. Hum. Mol. Genet. 23, 3467–3480.

Bharadwaj, R., Cunningham, K.M., Zhang, K., Lloyd, T.E., 2016. FIG4 regulates lysosome membrane homeostasis independent of phosphatase function. Hum. Mol. Genet. 25, 681–692. https://doi.org/10.1093/hmg/ddv505.

Charlesworth, G., Balint, B., Mencacci, N.E., Carr, L., Wood, N.W., Bhatia, K.P., 2016. SLC25A46 mutations underlie progressive myoclonic ataxia with optic atrophy and neuropathy. Mov. Disord. 31, 1249–1251. https://doi.org/10.1002/mds.26716.

Chow, C.Y., Reiter, L.T., 2017. Etiology of human genetic disease on the fly. Trends Genet. TIG 33, 391–398. https://doi.org/10.1016/j.tig.2017.03.007.

Haitina, T., Lindblom, J., Renström, T., Fredriksson, R., 2006. Fourteen novel human members of mitochondrial solute carrier family 25 (SLC25) widely expressed in the central nervous system. Genomics 88, 779–790. https://doi.org/10.1016/j.ygeno.2006.06.016.

Hediger, M.A., Romero, M.F., Peng, J.-B., Rolfs, A., Takanaga, H., Bruford, E.A., 2004. The ABCs of solute carriers: physiological, pathological and therapeutic implications of human membrane transport proteins. Pflã¼gers Arch. - Eur. J. Physiol. 447, 465–468. https://doi.org/10.1007/s00424-003-1192-y.

Janer, A., Prudent, J., Paupe, V., Fahiminiya, S., Majewski, J., Sgarioto, N., Des Rosiers, C., Forest, A., Lin, Z.-Y., Gingras, A.-C., Mitchell, G., McBride, H.M., Shoubridge, E.A., 2016. SLC25A46 is required for mitochondrial lipid homeostasis and cristae maintenance and is responsible for Leigh syndrome. EMBO Mol. Med. 8, 1019–1038. https://doi.org/10.15252/emmm.201506159.

Jantrapirom, S., Piccolo, L.L., Yoshida, H., Yamaguchi, M., 2018. (2017) A new *Drosophila* model of Ubiquilin knockdown shows the effect of impaired proteostasis on locomotive and learning abilities. Exp. Cell Res. 362, 461–471. https://doi.org/10.1016/j.yexcr.2017.12.010.

Keshishian, H., Broadie, K., Chiba, A., Bate, M., 1996. The drosophila neuromuscular junction: a model system for studying synaptic development and function. Annu. Rev. Neurosci. 19, 545–575. https://doi.org/10.1146/annurev.ne.19.030196.002553.

Klaus, S., Casteilla, L., Bouillaud, F., Ricquier, D., 1991. The uncoupling protein UCP: a membraneous mitochondrial ion carrier exclusively expressed in brown adipose tissue. Int. J. Biochem. 23 (9), 791–801.

Kyotani, A., Azuma, Y., Yamamoto, I., Yoshida, H., Mizuta, I., Mizuno, T., Nakagawa, M., Tokuda, T., Yamaguchi, M., 2016. Knockdown of the *Drosophila FIG4* induces deficient locomotive behavior, shortening of motor neuron, axonal targeting aberration, reduction of life span and defects in eye development. Exp. Neurol. 277, 86–95. https://doi.org/10.1016/j.expneurol.2015.12.011.

Lee, Y.S., Carthew, R.W., 2003. Making a better RNAi vector for *Drosophila*: use of intron spacers. Methods 30 (4), 322–329.

Li, Z., Peng, Y., Hufnagel, R.B., Hu, Y.C., Zhao, C., Queme, L.F., Khuchua, Z., Driver, A.M., Dong, F., Lu, Q.R., 2017. Loss of SLC25A46 causes neurodegeneration by affecting mitochondrial dynamics and energy production in mice. Hum. Mol. Genet. 26, 3776–3791. https://doi.org/10.1093/hmg/ddx262.

Li, J., Suda, K., Ueoka, I., Tanaka, R., Yoshida, H., Okada, Y., Okamoto, Y., Hiramatsu, Y., Takashima, H., Yamaguchi, M., 2019. Neuron-specific knockdown of *Drosophila HADHB* induces a shortened lifespan, deficient locomotive ability, abnormal motor neuron terminal morphology and learning disability. Exp. Cell Res. 379 (2), 150–158.

Menon, K.P., Carrillo, R.A., Zinn, K., 2013. Development and plasticity of the *Drosophila* larval neuromuscular junction. Wiley Interdiscip. Rev. Dev. Biol. 2, 647–670.

Muraoka, Y., Nakamura, A., Tanaka, R., Suda, K., Azuma, Y., Kushimura, Y., Piccolo, L.L., Yoshida, H., Mizuta, I., Tokuda, T., Mizuno, T., 2018. Genetic screening of the genes interacting with *Drosophila FIG4* identified a novel link between CMT-causing gene and long noncoding RNAs. Exp. Neurol. 310 (2018), 1–13. https://doi.org/10.1016/j.expneurol.2018.08.009.

Nelson, S.F., Koehler, C.M., Jen, J.C., 2016. Loss of function of SLC25A46 causes lethal congenital pontocerebellar hypoplasia. Brain 139, 2877–2890. https://doi.org/10.1093/brain/aww212.

Nguyen, M., Boesten, I., Hellebrekers, D.M., Mulder-den Hartog, N.M., de Coo, I.F., Smeets, H.J., Gerards, M., 2017. Novel pathogenic SLC25A46 splice-site mutation causes an optic atrophy spectrum disorder. Clin. Genet. 91, 121–125. https://doi.org/10.1111/cge.12774.

Niehues, S., Bussmann, J., Steffes, G., Erdmann, I., Köhrer, C., Sun, L., Wagner, M., Schäfer, K., Wang, G., Koerdt, S.N., Stum, 2016. Corrigendum: impaired protein translation in *Drosophila* models for charcot-marie-tooth neuropathy caused by mutant tRNA synthetases. Nat. Commun. 7, 10497. https://doi.org/10.1038/ncomms10497.

Nussbaum-Krammer, C.I., Neto, M.F., Brielmann, R.M., Pedersen, J.S., Morimoto, R.I., 2015. Investigating the spreading and toxicity of prion-like proteins using the metazoan model organism C. elegans. J. Vis. Exp. 95, 52321.

Palmieri, F., 2013. The mitochondrial transporter family SLC25: identification, properties and physiopathology. Mol. Aspects Med. 34, 465–484. https://doi.org/10.1016/j.mam.2012.05.005.

Pilling, A.D., Horiuchi, D., Lively, C.M., Saxton, W.M., 2006. Kinesin-1 and Dynein are the primary motors for fast transport of mitochondria in *Drosophila* motor axons. Mol. Biol. Cell 17, 2057–2068. https://doi.org/10.1091/mbc.E05-06-0526.

Rask-Andersen, M., Masuram, S., Fredriksson, R., Schiöth, H.B., 2013. Solute carriers as drug targets: current use, clinical trials and prospective. Mol. Aspects Med. 34, 702–710. https://doi.org/10.1016/j.mam.2012.07.015. The ABCs of membrane transporters in health and disease (SLC series).

Robinson, A.J., Kunji, E.R., 2006. Mitochondrial carriers in the cytoplasmic state have a common substrate binding site. Proc. Natl. Acad. Sci. U. S. A. 103 (8), 2617–2622.

Rocha, S., Freitas, A., Guimaraes, S.C., Vitorino, R., Aroso, M., Gomez-Lazaro, M., 2018. Biological implications of differential expression of mitochondrial-shaping proteins in Parkinson's disease. Antioxidants 7 (1), 1.

Sandoval, H., Yao, C.K., Chen, K., Jaiswal, M., Donti, T., Lin, Y.Q., Bayat, V., Xiong, B., Zhang, K., David, G., Charng, W.L., Yamamoto, S., Duraine, L., Graham, B.H., Bellen, 2014. Mitochondrial fusion but not fission regulates larval growth and synaptic development through steroid hormone production. eLife 3. https://doi.org/10.7554/eLife.03558.

Shimamura, M., Kyotani, A., Azuma, Y., Yoshida, H., Nguyen, T.B., Mizuta, I., Yoshida, T., Mizuno, T., Nakagawa, M., Tokuda, T., Yamaguchi, M., 2014. Genetic link between Cabeza, a*Drosophila* homologue of Fused in Sarcoma (FUS), and the EGFR signaling pathway. Exp. Cell Res. 326, 36–45.

Steffen, J., Vashisht, A.A., Wan, J., Jen, J.C., Claypool, S.M., Wohlschlegel, J.A., Koehler, C.M., 2017. Rapid degradation of mutant SLC25A46 by the ubiquitin-proteasome system results in MFN1/2-mediated hyperfusion of mitochondria. Mol. Biol. Cell 28, 600–612. https://doi.org/10.1091/mbc.E16-07-0545.

Storkebaum, E., Leitão-Gonçalves, R., Godenschwege, T., Nangle, L., Mejia, M., Bosmans, I., Ooms, T., Jacobs, A., Van Dijck, P., Yang, X.L., Schimmel, P., Norga, K., Timmerman, V., Callaerts, P., Jordanova, A., 2009. Dominant mutations in the tyrosyl-tRNA synthetase gene recapitulate in *Drosophila* features of human Charcot-Marie-Tooth neuropathy. Proc. Natl. Acad. Sci. U. S. A. 106, 11782–11787. https://doi.org/10.1073/pnas.0905339106.

Suda, K., Ueoka, I., Azuma, Y., Muraoka, Y., Yoshida, H., Yamaguchi, M., 2018. Novel *Drosophila* model for mitochondrial diseases by targeting of a solute carrier protein SLC25A46. Brain Res. 1689, 30–44. https://doi.org/10.1016/j.brainres.

Suda, K., Muraoka, Y., Ortega-Yáñez, A., Yoshida, H., Kizu, F., Hochin, T., Kimura, H., Yamaguchi, M., 2019. Reduction of *Rpd3* suppresses defects in locomotive ability and neuronal morphology induced by the knockdown of Drosophila SLC25A46 via an epigenetic pathway. Exp. Cell Res. 385 (2), 2019. https://doi.org/10.1016/j.yexcr.2019.111673. 111673.

Takahashi, Y., Hirose, F., Matsukage, A., Yamaguchi, M., 1999. Identification of three conserved regions in the DREF transcription factors from *Drosophila melanogaster* and *Drosophila virilis*. Nucleic Acids Res. 27 (2), 510–516.

Traba, J., Satrústegui, J., del Arco, A., 2009. Transport of adenine nucleotides in the mitochondria of Saccharomyces cerevisiae: interactions between the ADP/ATP carriers and the ATP-Mg/Pi carrier. Mitochondrion 9 (2), 79–85.

Wan, J., Steffen, J., Yourshaw, M., Mamsa, H., Andersen, E., Rudnik-Schöneborn, S., Pope, K., Howell, K.B., McLean, C.A., Kornberg, A.J., Joseph, J., Lockhart, P.J., Zerres, K., Ryan, M.M., Nelson, S.F., Koehler, C.M., Jen, J.C., 2016. Loss of function of SLC25A46 causes lethal congenital pontocerebellar hypoplasia. Brain 139, 2877–2890. https://doi.org/10.1093/brain/aww212.